

Article

Fluid Inclusion Constrained Multiple Petroleum Chargings in the Lithologic Reservoirs of the Late Eocene Shahejie Formation in the Minfeng Sag, Bohai Bay Basin, East China

Chunquan Li ^{1,2,*} , Honghan Chen ^{1,2} and Huimin Liu ³

¹ Key Laboratory of Tectonics and Petroleum Resources (China University of Geosciences), Ministry of Education, Wuhan 430074, China; hhchen@cug.edu.cn

² Department of Petroleum Geology, School of Earth Resources, China University of Geosciences (Wuhan), Wuhan 430074, China

³ Oil and Gas Exploration Management Center of Shengli Oilfield Branch Company Ltd., SINOPEC, Dongying 257015, China; hmliu@vip.163.com

* Correspondence: chunquanli@cug.edu.cn

Abstract: The fluid inclusion technique was utilized to reveal the petroleum charging events in the lithologic reservoirs embraced in the Late Eocene Shahejie Formation of the Minfeng sag, Bohai Bay Basin, East China. Petrography, fluorescence microspectrometry, and microthermometry were systematically carried out on 15 double-polished thin sections handled from reservoir core samples of the third Member of the Shahejie Formation. The results show that three generations of petroleum inclusions with fluorescence colors of yellow, yellowish green and bright blue were entrapped along the healed fractures in detrital quartz grains of these samples. The fluorescence features of petroleum inclusions illustrate that inclusion oils have different maturities and were products of source rocks at different stages. In addition, the trapping time of petroleum inclusions was determined by combining the homogenization temperatures of their coeval aqueous inclusions with thermal-burial histories. By integrating the petrographic occurrence, characteristics of petroleum inclusions, and the maturity and the trapping time of the studied inclusion oils, it is jointly constrained that the lithologic reservoirs of the Late Eocene Shahejie Formation in the Minfeng sag underwent three petroleum chargings, which occurred during 37.8~25 Ma, 11.7~3.5 Ma and 1.4~0.1 Ma, respectively. The petroleum from each charging period migrated from the center of the sag to the edge, and the lower the maturity of the migrating petroleum, the longer the migration duration.

Keywords: fluid inclusion; fluorescence microspectrometry; microthermometry; hydrocarbon charging history; minfeng sag; Bohai Bay Basin



Citation: Li, C.; Chen, H.; Liu, H. Fluid Inclusion Constrained Multiple Petroleum Chargings in the Lithologic Reservoirs of the Late Eocene Shahejie Formation in the Minfeng Sag, Bohai Bay Basin, East China. *Energies* **2022**, *15*, 3682. <https://doi.org/10.3390/en15103682>

Academic Editor: Reza Rezaee

Received: 21 February 2022

Accepted: 13 May 2022

Published: 17 May 2022

Publisher's Note: MDPI stays neutral with regard to jurisdictional claims in published maps and institutional affiliations.



Copyright: © 2022 by the authors. Licensee MDPI, Basel, Switzerland. This article is an open access article distributed under the terms and conditions of the Creative Commons Attribution (CC BY) license (<https://creativecommons.org/licenses/by/4.0/>).

1. Introduction

The determination of reservoir charging events has been one of the most important aspects of hydrocarbon exploration and exploitation, especially when there is a need to reconstruct the dynamic processes of hydrocarbon accumulation. Researchers have developed many methods to reveal the hydrocarbon charging events for a reservoir [1–7], and among these methods, fluid inclusion is a widely used and highly efficient technique [8–13]. A tiny fluid inclusion is the original sample of palaeofluid and was widely used as a geothermometer and geobarometer to reconstruct the temperature and pressure conditions of the geological time at which it formed [14–16]. In addition, with the advances in test methodology and renovations in experiment facilities [17–22], fluid inclusions can provide tremendous micro information at a low cost about the palaeofluids for which they stand. When the palaeofluids are petroleum, four types of data for petroleum inclusions can be revealed through analysis and modeling: (1) textures (which give indirect information on the time aspect), (2) fluid composition, (3) pressure-volume-temperature (PVT) properties and

(4) pressure-temperature (PT) of trapping, according to the statements of Munz (2001) [23]. These valuable data make petroleum inclusion a powerful tool to trace hydrocarbon evolution (generation-migration-accumulation) during the geological time [24–30]. Thus, the fluid inclusion technique, especially the application of petroleum inclusions, is preferably adopted by oil companies and individual researchers.

Fluid inclusions were used in some past research works on the Dongying depression, Bohai Bay Basin, East China. Cai et al. (2009) reconstructed the paleofluid potential field of the third Member of the Shahejie Formation of the Dongying depression with systematic fluid inclusion analysis [31]. Liu (2009) studied the pressure evolution of the third Member of the Shahejie Formation in the Minfeng sag of the Dongying depression by thermal dynamic modeling with fluid inclusions [32]. Ping et al. (2017) discussed petroleum accumulation in the deeply buried reservoirs in the northern part of the Dongying depression using fluid inclusions collaborated with natural gas geochemistry and 1-D basin modeling [33]. However, there are few works using fluid inclusions to reveal petroleum charging events of a reservoir in the Dongying depression, especially of a lithologic reservoir. Recently, some detailed investigations in the Dongying depression [34,35] show great potential in lithologic reservoir exploration, especially in the Late Eocene Shahejie Formation. Oil companies are eager to understand the dynamic processes of hydrocarbon migration and accumulation for the lithologic reservoirs; hence it has become a growing interest for petroleum geologists to study the petroleum charging histories of lithologic reservoirs in the whole depression. In this study, the fluid inclusion technique was employed to constrain the petroleum charging events of lithologic reservoirs in the third Member of the Late Eocene Shahejie Formation in the Minfeng sag. That is, to investigate how many episodes of and when the petroleum chargings happened in the lithologic reservoirs so that a further understanding of the dynamic processes of hydrocarbon migration and accumulation in the Minfeng sag can be achieved.

2. Geological Setting

The Bohai Bay Basin, one of the most important hydrocarbons producing basins in China, is located on the eastern coast of China, with an area of approximately 200,000 km² (Figure 1a). It was developed on Archean and Proterozoic basement of the North China Craton during the Late Cretaceous and evolved into an intracratonic rift basin of several sub-basins during the Cenozoic [36–38]. This tectonic evolution includes two distinct stages: a syn-rifting stage (65–24.6 Ma) and a post-rifting stage (24.6–0 Ma) (Figure 2) [39]. The syn-rifting stage is composed of four sub-stages: the initial (stage I), the expansion (stage II), the expansion and deep subsiding (stage III) and the contraction (stage IV) [37]. The syn-rifting sediments were deposited in lacustrine environments and restricted to the grabens and half grabens [40,41], while the post-rifting sediments are dominated by fluvial deposits [42,43].

As a part of the Jiyang sub-basin, the Dongying depression was formed as a result of Tertiary rifting, and the sedimentary filling of the Tertiary sequence is composed of five formations: the Paleocene-Eocene Kongdian Formation (Ek), the Eocene-Oligocene Shahejie Formation (Es), the Oligocene Dongying Formation (Ed), the Miocene Guantao Formation (Ng) and the Miocene-Pliocene Minghuazhen Formation (Nm) (Figure 2). The entire Tertiary sequence is lithologically dominated by non-marine sandstones and mudstones with subordinate carbonates and evaporates, which make up a complex stacking pattern of source rocks, reservoir formations and seal rocks. Hydrocarbons discovered currently in the Dongying depression are mainly sourced from and mostly reservoirized in the Tertiary strata, especially the Shahejie Formation [44]. The Shahejie Formation comprises four Members (Es₄, Es₃, Es₂, and Es₁) from the base upwards. The third Member (Es₃) is further divided into three parts marked as Es₃^L (the lower part), Es₃^M (the middle part) and Es₃^U (the upper part), while the fourth Member (Es₄) is divided into two parts marked as Es₄^U (the upper part) and Es₄^L (the lower part). The Es₃^L and the Es₄^U are the two most important source

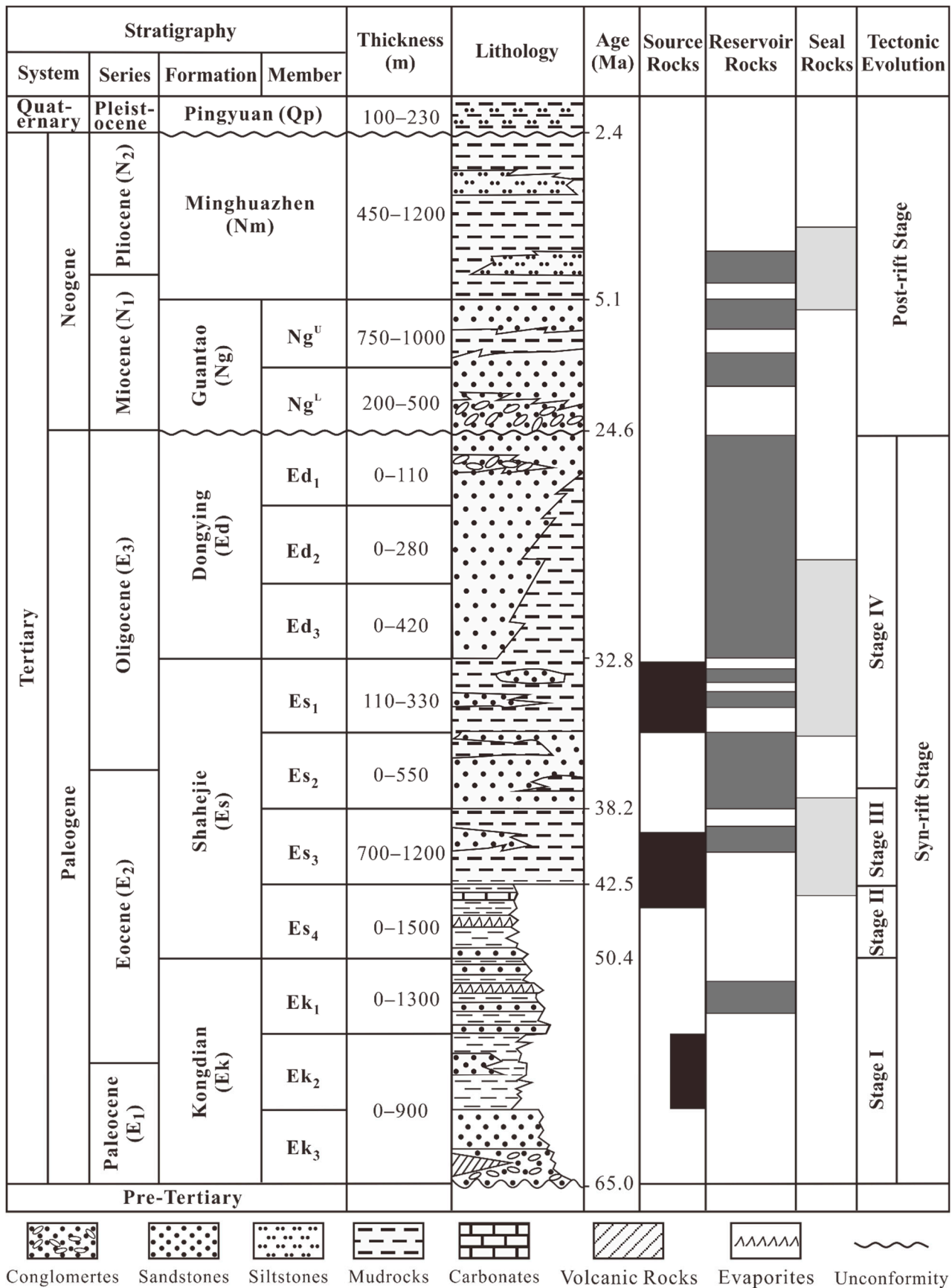


Figure 2. The Tertiary stratigraphy of the Dongying depression.

The Dongying depression is subdivided into four sags named the Boxing sag, the Niuzhuang sag, the Lijin sag and the Minfeng sag. The Minfeng sag is the smallest one, with an area of approximately 200 km², and is located at the most northeast part of the Dongying depression (Figure 1b). Its formation and tectonic evolution were dominated by three groups of fault systems (Figure 1c). Within the sag, the whole Tertiary strata were deposited, but parts of them are missing at the edge. Exploration in the Minfeng sag has clearly revealed structural reservoirs, but for the lithologic reservoirs embraced in the third Member of the Shahejie Formation, the study is not as adequate as the other three sags.

3. Samples and Methods

3.1. Samples

Fifteen reservoir core samples were collected from eight wells in the Minfeng sag, including five samples from wells located at the edge of the sag and ten samples from wells in the center of the sag (Figure 1c, Table 1). All fifteen samples are from the third Member of the Shahejie Formation (Es₃) and lithologically are mainly fine-grained sandstone and siltstone. Doubly polished thin sections about 100 µm thick were prepared from all the samples to perform fluid inclusion studies, including petrography, fluorescence microspectrometry and microthermometry.

3.2. Petrography

Petrographic examination of a sample is the first and essential step of any fluid inclusion study [45]. All of the fifteen doubly polished thin sections were carefully examined under a two-channeled Nikon 80i microscope. By shifting between the transmitted light and the ultraviolet (UV) light, petroleum inclusions were readily distinguished from aqueous inclusions based on the fluorescing feature of inclusion oils [23]. Moreover, characteristics of their shape, size and distribution were recorded. During this procedure, the fluid inclusion assemblage (FIA) method [46] was carefully implemented, and some common problems and pitfalls [47] were overcome to make sure that only inclusions trapped at the same time and under the same set of diagenetic conditions were used for systematic analysis.

3.3. Fluorescence Microspectrometry

Fluorescence microspectrometry was carried out on petroleum inclusions with different fluorescence colors through the Ocean Optics Maya 2000 Pro spectrometer mounted on the Nikon 80i microscope. The incident UV light is of 365 nm wavelength, and the spectra of the emitted visible light are between 400~700 nm wavelength; hence the spectrometer is set to record the spectrum range of 300~1000 nm for this study. Meanwhile, a computer-assisted color testing technique was utilized with the help of Yuanao software to avoid naked eye errors in fluorescence color identification. Subsequently, some common quantitative parameters such as λ_{\max} , QF-535 and $Q_{650/500}$ [23] were used to characterize the spectra.

3.4. Microthermometry

Microthermometry was performed both on petroleum inclusions and their coeval aqueous inclusions to determine their homogenization temperatures (T_{hs}) by using a Linkam THMS G600 heating/cooling stage mounted on the Nikon 80i microscope. The stage has been calibrated with synthetic fluid inclusions. In order to get reliable homogenization temperatures, the heating rate was programmed at 10 °C/min during the initial stage of each heating run, reduced to 1 °C/min when it is close to the homogenization temperature, and then maintained till the final homogenization. During the entire procedure, inclusions (either petroleum or aqueous) that showed obvious signs of necking down, stretching, leakage or refilling were excluded from the final microthermometry analysis [48].

Table 1. Sample information, occurrence and fluorescence property of typical petroleum inclusions.

| Well | Sample # | Depth (m) | Lithology | Location | FluorescenceColor | λ_{\max} (nm) | QF-535 | Q _{650/500} | Mean T _h (°C) | |
|-----------|----------|-----------|-----------|-----------------|-------------------|-----------------------|-----------|----------------------|--------------------------|----------------|
| | | | | | | | | | Petroleum | Coeval Aqueous |
| Yan182 | 1 | 2222.30 | MCS | FWQG | Yellow | 575.5–586.3 | 2.25–3.67 | 0.87–1.67 | 91.5 | 97.7 |
| | | | | FTQG | Yellowish green | 536.4–545.4 | 1.80–2.06 | 0.65–0.88 | 105.5 | 115.8 |
| | 2 | 2264.20 | FS | FTQG and FWQG | Bright blue | 492.9–494.3 | 1.12–1.29 | 0.38–0.51 | 151.0 | |
| Yan18 | 3 | 2279.95 | CFS | FWQG | Yellowish green | 543.1–545.9 | 1.37–2.15 | 0.50–0.87 | 105.8 | 115.2 |
| | | | | FTQG | Yellow | 589.0 | 2.61 | 1.09 | 98.2 | 113.8 |
| | | | | FTQG | Yellowish green | 546.8–549.0 | 1.73–2.13 | 0.66–0.90 | 125.5 | |
| Yan18 | 4 | 2265.40 | FS | FTQG | Yellowish green | 542.7–543.6 | 1.49–1.65 | 0.53–0.60 | 116.8 | 139.2 |
| Fengshen1 | 5 | 2865.60 | SC | FWQG | Yellow | 582.3 | 2.42 | 1.02 | 84.5 | 97.9 |
| | | | | FTQG | Yellowish green | 538.2 | 1.65 | 0.66 | 120.5 | 130.1 |
| Xinxie152 | 6 | 2548.50 | MCS | FTQG | Yellow | 584.5–587.2 | 3.10–3.14 | 1.39–1.43 | 87.3 | 101.0 |
| | 7 | 2582.90 | FS | FTQG | Yellowish green | 542.7 | 1.82 | 0.75 | 119.1 | 139.2 |
| Feng4 | 8 | 2748.60 | FS | FTQG and FWQG | Yellow | 578.7–584.5 | 2.38–3.47 | 0.96–1.64 | 84.9 | 101.1 |
| | | | | FTQG | Yellowish green | 545.0–551.3 | 1.56–2.09 | 0.61–0.81 | | |
| Feng14 | 9 | 2845.00 | SS | FTQG | Yellowish green | 538.6–543.6 | 1.42–2.0 | 0.59–0.87 | 108.6 | 114.6 |
| | 10 | 2846.10 | SS | FTQG | Bright blue | 491.6–493.4 | 0.78–1.06 | 0.27–0.40 | | |
| | | | | FTQG | Yellow | 576.9–585.8 | 2.28–2.41 | 0.97–1.01 | 79.5 | 91.5 |
| | 11 | 2848.20 | SS | FTQG | Yellowish green | 552.2 | 2.22 | 0.91 | | |
| | | | | FTQG | Yellowish green | 542.7–545.4 | 1.87–2.04 | 0.73–0.86 | 87.8 | 107.2 |
| | | | | FTQG and FWQG | Bright blue | 492.9 | 0.95 | 0.33 | 114.3 | 134.6 |
| Feng112 | 12 | 2896.40 | FS | FTQG | Yellow | 577.8–586.7 | 2.32–2.60 | 0.98–1.13 | 96.9 | 107.0 |
| | | | | FTQG | Yellowish green | 544.0 | 2.11 | 0.89 | 107.8 | 116.9 |
| | 13 | 3108.20 | FS | FTQG | Yellow | 579.1–580.9 | 2.33–2.59 | 0.94–1.08 | 87.5 | 100.0 |
| | | | | FTQG and FWQG | Yellowish green | 547.2 | 1.79 | 0.71 | 113.1 | 136.5 |
| | | | | FTQG and FWQG | Bright blue | 494.8 | 0.97 | 0.36 | 135.9 | 152.3 |
| 14 | 3108.80 | FS | FTQG | Yellowish green | 542.7 | 2.22 | 0.91 | 114.7 | 139.9 | |
| Ying544 | 15 | 3044.30 | FS | FWQG | Yellow | 586.3–588.5 | 2.80–2.87 | 1.21–1.23 | 85.4 | 98.7 |

Note: MCS-Moderate coarse sandstone; FS-Fine sandstone; CFS-Conglomeratic fine sandstone; SC-Sandy conglomerate; SS-Siltstone.

4. Results

4.1. Distribution and Characteristics of Petroleum and Coeval Aqueous Inclusions

Petrographic characterization results illustrated that abundant petroleum inclusions and aqueous inclusions were entrapped in these 15 samples (Figure 3, Table 1), and the coeval relationship between petroleum inclusions and aqueous inclusions was very clear (Figure 3j–l). Petroleum inclusions were found mainly trapped in the detrital quartz grains and rarely in cement and some other detrital grains, such as feldspar. In quartz grains, they are mostly distributed along the healed fractures, which are through the quartz grain (FTQG) or within the quartz grain (FWQG) (Figure 3, Table 1). In most cases, there are aqueous inclusions accompanying the petroleum inclusions, whereas in some cases, there are no coeval aqueous inclusions observed. The petroleum inclusions usually have irregular shapes with a size range of 1–20 μm (the largest one can reach 50 μm) and contain less than 15% vapor, whereas the coeval aqueous inclusions are usually in elliptical or spherical shapes with diameters in the range of 5–20 μm (the largest one can reach 30 μm), and contain less than 10% vapor.

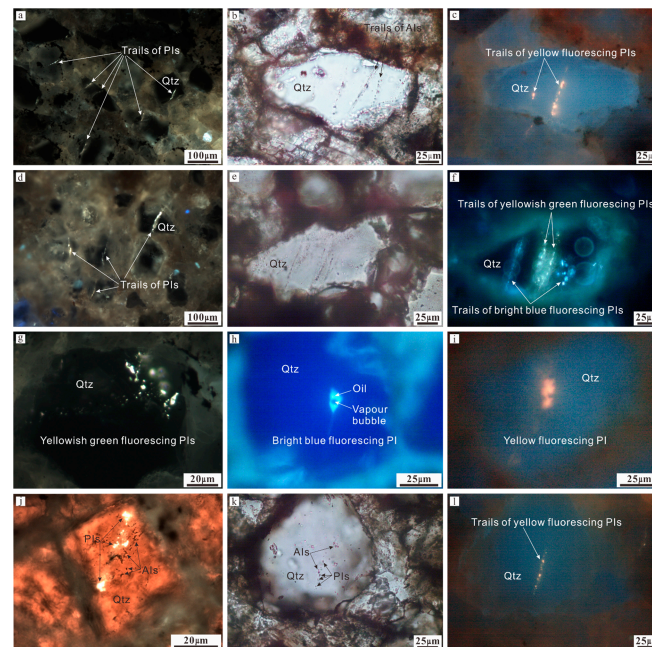


Figure 3. Series of photomicrographs showing the distribution of petroleum inclusions (PIs) and coeval aqueous inclusions (AIs) under the ultraviolet light (UV; a,c,d,f–j,l) and the transmitted light (TL; b,e,j,k) from the Es₃ reservoirs in the Minfeng sag, Bohai Bay Basin, East China. (a) shows trails of PIs along the healed fractures (both FTQG and FWQG) in quartz (Qtz), from well Feng4, 2748.60 m; (b,c) are the same field of view and show trails of yellow fluorescing PIs along the healed fractures (both FTQG and FWQG) in quartz, from Feng4, 2748.60 m; (d) shows trails of PIs along the healed fractures (both FTQG and FWQG) in quartz, from well Feng112, 2896.40 m; (e,f) are the same field of view and show trails of yellowish green and bright blue fluorescing PIs along the healed fractures (both FTQG and FWQG) in quartz, from well Feng14, 2848.20 m; (g) shows yellowish green fluorescing PIs along the healed fractures (both FTQG and FWQG) in quartz, from well Feng4, 2748.60 m; (h) shows the detail of a petroleum inclusion trapped along FWQG in quartz, with a vapour bubble and bright blue fluorescing oil, from well Feng14, 2848.20 m; (i) shows a yellow fluorescing petroleum inclusion trapped along FTQG in quartz, from well Feng4, 2748.60 m; (j) shows trail of yellowish green fluorescing PIs and their coeval AIs along the healed fracture (FTQG) in quartz, UV+TL, from well Feng4, 2748.60 m; (k,l) are the same field of view and show trail of yellow fluorescing PIs and coeval AIs along the healed fracture (FWQG) hosted in quartz, from well Feng4, 2748.60 m.

4.2. Fluorescence Colors and Microspectrometry of Petroleum Inclusions

Based on the visual determination of fluorescence colors during the identification of petroleum inclusions under UV light, three different fluorescence colors were assigned to petroleum inclusions among these 15 samples, and they are yellow (Figure 3c,i,l), yellowish green (Figure 3f,g,j) and bright blue (Figure 3f,h). The yellowish green fluorescing petroleum inclusions are the most common petroleum inclusion assemblages (PIAs) in these samples and were observed in 13 samples from all wells except well Ying544, while the yellow fluorescing PIAs were observed in nine samples from all wells except well Yan18, and the bright blue fluorescing PIAs were observed only in 4 samples from wells of Feng14, Feng112 and Yan182 (Table 1). Among these 15 samples, there are only 2 samples in which petroleum inclusions fluorescing yellow, yellowish green and bright blue were all detected. Moreover, there are seven samples in which petroleum inclusions with two kinds of fluorescence colors were detected; five of them trapped petroleum inclusions fluorescing yellow and yellowish green, two of them trapped petroleum inclusions fluorescing yellowish green and bright blue. In addition, petrographically, the yellow fluorescing petroleum inclusions are mainly limited in FWQG, while the yellowish green and bright blue fluorescing petroleum inclusions are mostly along FTQG (Figure 3, Table 1).

Fluorescence spectra of typical petroleum inclusions were obtained by microspectrometry for these fifteen samples and presented in Figure 4. The spectra shapes show that there are three main peak wavelength ranges corresponding to the three fluorescence colors we assigned. The most common yellowish green fluorescing petroleum inclusions have a main peak wavelength range of 536.4~551.3 nm, whereas the yellow fluorescing petroleum inclusions have a main peak wavelength range of 575.5~589.0 nm, and the bright blue fluorescing petroleum inclusions have a main peak wavelength range of 491.6~494.8 nm (Table 1). Among the eight sampling wells, all three ranges of main peak wavelengths were detected only in well Feng14, Feng112 and Yan182 (Figure 4a–c), and one or two ranges were seen in the other five wells (Figure 4d). The range of main peak wavelength for the bright blue fluorescence is relatively concentrated, and the yellow and the yellowish green fluorescence both have a dispersion of about 15 nm. This difference may be due to the different number of spectra obtained for the three fluorescence colors from the statistical point of view.

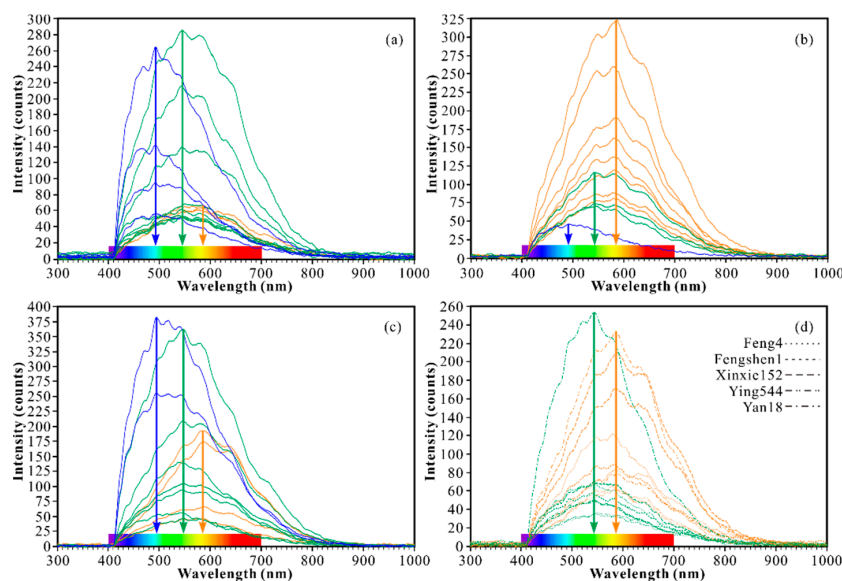


Figure 4. Fluorescence spectra of typical petroleum inclusions. (a) data from well Feng14; (b) data from well Feng112; (c) data from well Yan182; (d) data from wells of Feng4, Fengshen1, Xinxie152, Ying544 and Yan18.

The quantitative results of the fluorescence spectra are listed in Table 1. It shows that the QF-535 parameter for yellow, yellowish green and bright blue fluorescing petroleum inclusions is in the range of 2.25~3.67, 1.37~2.22 and 0.78~1.29, respectively, and the $Q_{650/500}$ parameter for yellow, yellowish green and bright blue fluorescing petroleum inclusions is in the range of 0.87~1.67, 0.5~0.91 and 0.27~0.51, respectively.

4.3. Microthermometry

Homogenization temperatures of 127 aqueous inclusions and 77 petroleum inclusions acquired from these 15 samples by microthermometry analysis are summarized in Figure 5. The results indicate that the homogenization temperatures of different fluorescing petroleum inclusions are a bit different in different wells. For yellow fluorescing petroleum inclusions, the measured T_h s are between 84.7 °C and 99.6 °C in well Feng112, between 74.9 °C and 89.5 °C in well Feng14, between 90.6 °C and 99.6 °C in well Yan182 and between 79.3 °C and 91.5 °C in the other five wells. For yellowish green fluorescing petroleum inclusions, the T_h s range is from 107.2 °C to 117.3 °C in well Feng112, from 105.7 °C to 115.3 °C in well Feng14, from 103.8 °C to 126.3 °C in well Yan182 and from 115.3 °C to 120.5 °C in the other five wells. For bright blue fluorescing petroleum inclusions, the T_h s are between 134.8 °C and 137.2 °C in well Feng112 and between 147.4 °C and 156.3 °C in well Yan182. Only one T_h data (114.3 °C) is acquired for bright blue fluorescing petroleum inclusions in well Feng14 due to the observation failure in the homogenization processes, and this T_h value seems odd, so we list it in Table 1, but it is not illustrated in Figure 5. In the other five wells, no bright blue fluorescing petroleum inclusions were detected; of course, there is no T_h obtained. Taking all the T_h data into account, the three generations of petroleum inclusions which are respectively fluorescing yellow, yellowish green and bright blue have focus T_h modes in the 85–100 °C, 110–120 °C and 140–150 °C classes, and have mean T_h s of 87.3 °C, 112.7 °C and 145.3 °C, respectively.

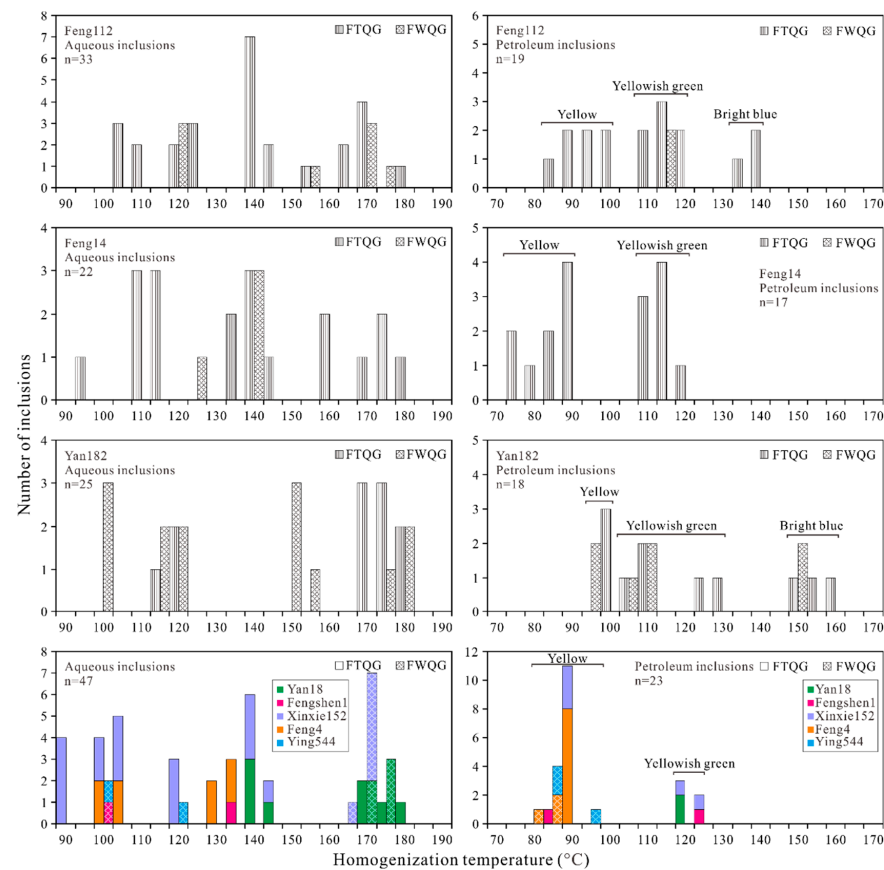


Figure 5. The homogenization temperature histograms of aqueous and petroleum inclusions.

T_h s of coeval aqueous inclusions of the yellow, yellowish green and bright blue fluorescing petroleum inclusions are also a bit different in different wells (Figure 5). In well Feng112, the T_h s are respectively between 103.2 °C and 124.5 °C, between 136.4 °C and 141.7 °C and between 153.2 °C and 176.1 °C. In well Feng14, the T_h s are respectively between 94.7 °C and 113.5 °C, between 124.9 °C and 141.3 °C and between 156.1 °C and 175.3 °C. In well Yan182, the T_h s are respectively between 96.8 °C and 116.3 °C, between 145.8 °C and 155.0 °C and between 168.3 °C and 177.2 °C. In the other five wells, the T_h s of coeval aqueous inclusions of yellow and yellowish green fluorescing petroleum inclusions range from 85.6 °C to 103.5 °C and from 118.3 °C to 140.2 °C, respectively, and another group of aqueous inclusions we measured have the T_h between 164.3 °C and 174.5 °C, similar to T_h s of the coeval aqueous inclusions of bright blue fluorescing petroleum inclusions which are observed in wells of Feng112, Feng14 and Yan182. Considering all the T_h data, coeval aqueous inclusions of the yellow, yellowish green and bright blue fluorescing petroleum inclusions have focus T_h modes in the 100–120 °C, 130–145 °C and 165–175 °C classes and have mean T_h s of 107.4 °C, 139.4 °C and 168.4 °C respectively.

By comparison, the microthermometry results also suggest that the homogenization temperature of each generation of petroleum inclusions is usually 10–20 °C lower than that of their corresponding coeval aqueous inclusions (Table 1).

5. Discussions

5.1. Indication of Fluid Inclusion Petrography on Petroleum Chargings

Fluid inclusions are the original samples of palaeofluids; hence the occurrence of petroleum inclusions indicates the processes of hydrocarbon generation, migration and accumulation [23,29]. A large amount of petroleum inclusions entrapped in the sandstone reservoir of the Late Eocene Shahejie Formation (Es_3) verified that the Es_3 lithologic reservoirs underwent petroleum charging processes during the geologic time. The stage and relative time sequence of petroleum chargings can be revealed by the distribution and intersectional relation between fluid inclusions [45,49]. All petroleum inclusions observed in the Es_3 reservoirs of the Minfeng sag occurred along the healed fractures (both FTQG and FWQG) in detrital quartz grains (Figure 3); hence we can deduce that the petroleum charging is related to the forming of fractures in the Es_3 sandstone reservoir. Previous research works suggest that fractures in the Es_3 sandstone reservoirs result from strong compaction and overpressure accumulated during oil generation at the late stage of diagenesis [50]. Therefore, according to the petrographic criteria of fluid inclusions, the widespread petroleum inclusions are secondary, and along with their relationships to the diagenetic sequence, it is clearly reflected that the petroleum chargings happened in the late diagenetic stage. Moreover, Liu (2009) pointed out that the overpressure evolution in the Es_3 reservoirs of the Minfeng sag experienced three cycles of pressure increasing and decreasing [32], which resulted in multi-stage fracturing. Consequently, we can boldly infer that there are multiple petroleum chargings existing in the Es_3 lithologic reservoirs of the Minfeng sag. The petroleum inclusions with different fluorescence colors and their distribution difference that the yellow fluorescing petroleum inclusions are mainly limited in FWQG while the yellowish green and bright blue fluorescing petroleum inclusions are mostly along FTQG, strongly evidenced our inference.

5.2. Maturity of Inclusion Oils and Its Indication on Petroleum Chargings

The maturity of organic matter is traditionally characterized by geochemical parameters such as T_{max} in Rock Eval pyrolysis [51] and sterane or hopane biomarker ratios [52]. Using fluorescence property to quantitatively reflect the maturity of crude oils was studied and has been extrapolated to inclusion oils [53–56]. This unconventional method underwent some outstanding and valuable discussions around the relationship between fluorescence color and thermal maturity [57–62]. Currently, it is widely accepted that the blue fluorescence color is associated with high maturity, whereas the yellow and orange fluorescence colors correlate to relatively low maturity [1,12,54]. Oxtoby (2002) pointed out

in his comments [58] on George et al.'s work [57] that a standard color chart should be used to avoid naked-eye errors when identifying the fluorescence colors. Our computer-assisted color testing results shown in the chromaticity diagram (Figure 6a) display a remarkable distinction among three fluorescence colors, and all results are consistent with the color assignment by our naked eyes. Based on these, the yellow fluorescing petroleum inclusions trapped in the E_{s3} reservoirs of the Minfeng sag enclosed oils with relative lower maturity, and the bright blue fluorescing petroleum inclusions enclosed oils with relatively higher maturity. The maturity of the oils enclosed in yellowish green fluorescing petroleum inclusions is somewhere in between.

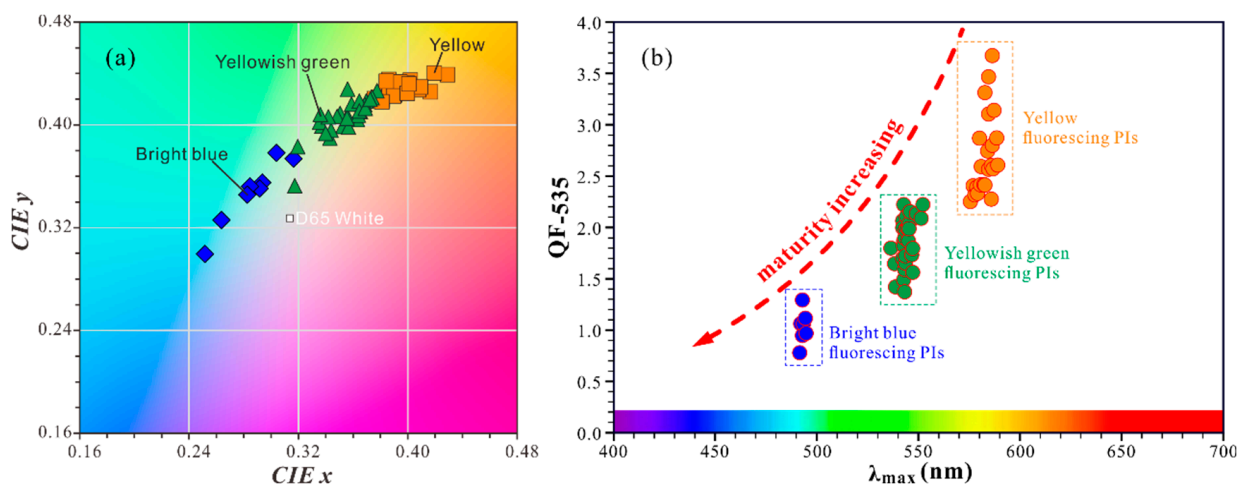


Figure 6. Chromaticity diagram (a) and spectrum parameters plots of QF-535 versus λ_{max} (b) of petroleum inclusions.

The fluorescence spectrum and the quantitative parameters were also used to characterize the relative maturity of crude oils and inclusion oils [17,23,54,61]. Researchers carried out theoretical and experimental studies and generally found that the main peak wavelength (λ_{max}) shifts toward a longer wavelength with the decrease of maturity (a redshift) and toward a shorter wavelength with the increase of maturity (a blueshift) [53,63]. Correspondingly, the quantitative parameters of QF-535 and $Q_{650/500}$ decrease with increasing maturity [53,54]. Figure 4 demonstrates a considerable wavelength shift from the longer to the shorter from yellow to yellowish green and bright blue fluorescing petroleum inclusions. These shifts suggest that in the E_{s3} lithologic reservoirs of the Minfeng sag, the oils trapped in yellow fluorescing petroleum inclusions have relatively lower maturity, and the oils trapped in bright blue fluorescing petroleum inclusions have relatively higher maturity. The values of QF-535 and $Q_{650/500}$ of bright blue fluorescing petroleum inclusions are smaller than that of yellowish green fluorescing petroleum inclusions and much smaller than that of yellow fluorescing petroleum inclusions (Table 1, Figure 6b), which also shows that oils trapped in petroleum inclusions in the E_{s3} lithologic reservoirs of the Minfeng sag have different maturity.

According to Liu et al. (2009), the source of the lithologic reservoirs in the third Member of the Shahejie Formation is mainly from the continuous formations of E_{s3}^L and E_{s4}^U and dominantly from the formation of E_{s3}^L [44]. Different maturities form an evolutionary sequence, and the evolution trend of maturity is sketched in Figure 6b based on the changes in the main peak wavelength and QF-535 parameter. Moreover, it can be confirmed that the different maturities of inclusion oils represent the supplies from the source at different stages, which was supported by the microthermometry results. The petroleum inclusions with different fluorescence colors have different homogenization temperatures, and so are their coeval aqueous inclusions (Table 1, Figure 5). Therefore, the spreading of the inclusion

of oil maturity implies multiple petroleum chargings underwent in the Es₃ lithologic reservoirs of the Minfeng sag, and each charging occurred at a separate stage.

5.3. Episodes and Time of Petroleum Chargings

Integration of fluid inclusion petrography and petroleum inclusion characteristics suggest that petroleum chargings in the Es₃ lithologic reservoirs of the Minfeng sag are relatively late, and there are multiple charging stages. According to the correlation between fluorescence properties and microthermometry results, three episodes of petroleum chargings occurred in the geological time.

The timing of a petroleum charging event can be solved by some direct and traditional ways, such as isotopic dating [6] and basin modeling [64]. Using fluid inclusion to determine time is an indirect method, which must be combined with the thermal-burial history. Hence, the one-dimensional module of software BasinMod was used to reconstruct the thermal-burial histories for the eight sampling wells. Detail parameter assignment and model choosing are following Ping et al.'s related work on the Dongying depression [33]. The trapping time of the petroleum inclusion, which stands for the petroleum charging time, was determined one by one (Figure 7) by projecting the homogenization temperatures of aqueous inclusions, which are coeval with petroleum inclusions [10,23] onto palaeogeothermal burial curves.

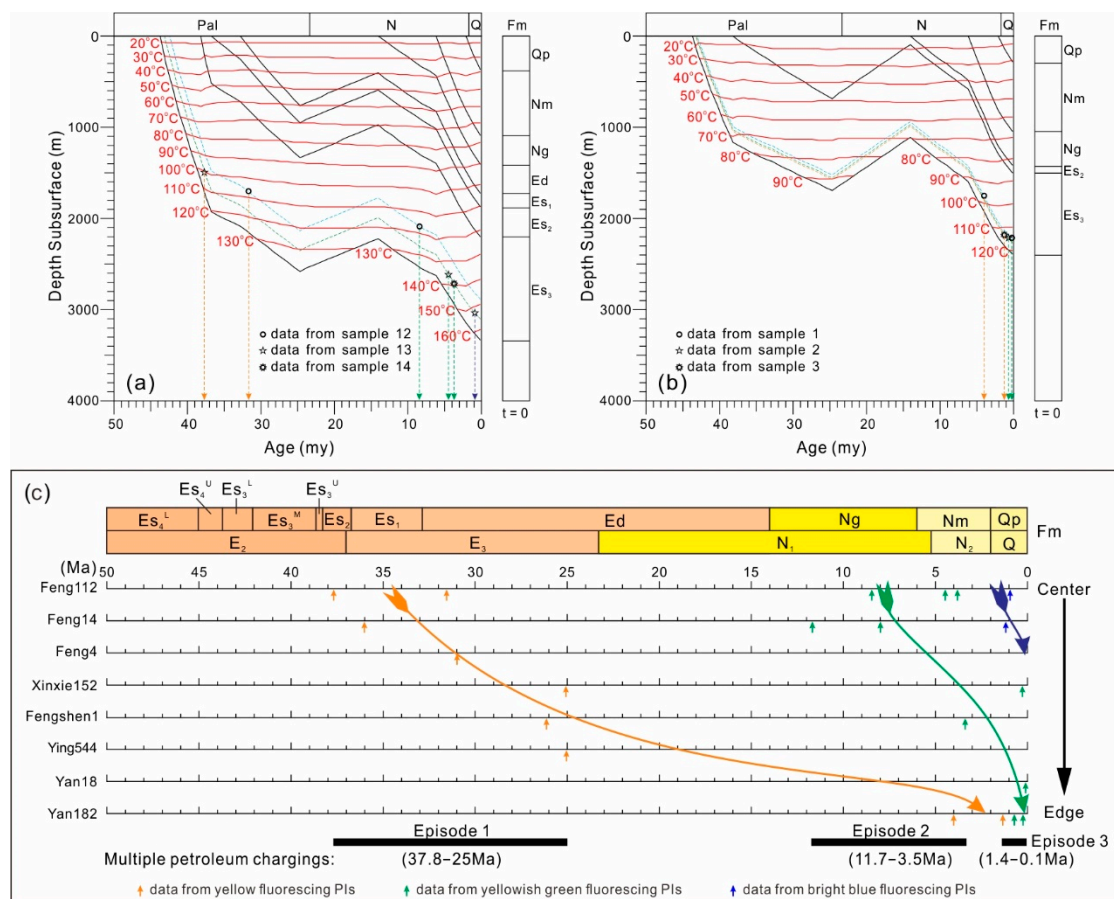


Figure 7. Determination of the hydrocarbon charging episodes and the corresponding time. (a) Timing the petroleum chargings in the well Feng112, located in the center of the sag; (b) timing the petroleum chargings in the well Yan182, located at the edge of the sag; (c) classifying the petroleum charging episodes by integrating all the time data gotten from all the wells.

Although oils within petroleum inclusions from the same generation tend to have the same fluorescence color, the absolute charging time varies in eight sampling wells, but all display a trend of getting later from the center of the Minfeng sag to the edge (Figure 7c). This is correlated to the distribution of source rocks and the result of petroleum migration as well. Mature source rocks of the Minfeng sag were limited in the center part of the sag [44,65]; the generated petroleum certainly charges the closest lithologic traps first and then those farther away after a period of migration. Figure 7a,b show the determined trapping time of petroleum inclusions in the well Feng112, which is located in the center of the Minfeng sag and the well Yan182, which is located at the edge. The burial depth of the Es₃ reservoir is much shallower in well Yan182 than that in well Feng112; hence the direct Es₃^L source matured much earlier in well Feng112 than well Yan182 according to the theory of hydrocarbon generation. Consequently, the petroleum charging times in the center and at the edge of the Minfeng sag are obviously different. Taking all the trapping times into consideration from the time point of view, the three episodes of petroleum chargings in the Es₃ lithologic reservoirs of the Minfeng sag occurred during 37.8–25 Ma, 11.7–3.5 Ma and 1.4–0.1 Ma, respectively (Figure 7c).

Since the maturity of the Es₃^L source rocks varies in different locations of the Minfeng sag, the migration trends of the three petroleum generations marked with yellow, yellowish green and bright blue fluorescing petroleum inclusions are also different, as illustrated in Figure 7c. It can be inferred that the petroleum in the Minfeng sag migrated from the center to the edge, and for each generation, the migration period varies as petroleum comes with different maturity. The lower the maturity, the longer the migration time or the wider the migration window. For example, the yellow fluorescing inclusion oils have the lowest maturity, hence take the longest time to migrate.

6. Conclusions

Recent work shows great exploration potential for lithologic reservoirs in the Late Eocene Shahejie Formation of the Minfeng sag, and multiple petroleum chargings in the Es₃ lithologic reservoirs were constrained by systematic fluid inclusion analysis in this study.

Three generations of petroleum inclusions, fluorescing yellow, yellowish green and bright blue, were entrapped in the healed fractures (including FTQG and FWQG) of the detrital quartz grains of the Es₃ lithologic reservoirs. Moreover, petrographically, the yellow fluorescing petroleum inclusions are mainly found in FWQG, while the yellowish green and bright blue fluorescing petroleum inclusions are mostly in FTQG, which suggests that the yellow fluorescing petroleum inclusions are entrapped earlier than the yellowish green and bright blue fluorescing petroleum inclusions.

Fluorescence colors, spectrum properties and the quantitative parameters all illustrate that the inclusion oils fluorescing yellow have relative lower maturity while the inclusion oils fluorescing bright blue have relative higher maturity, and the inclusion oils fluorescing yellowish green have the maturity somewhere in between.

These three generations of oils with different fluorescence colors are a series of supplies from the Es₃^L source rocks at different stages. Indirect dating with fluid inclusions suggested that the Es₃ lithologic reservoirs of the Minfeng sag experienced three episodes of petroleum chargings, and they occurred during 37.8–25 Ma, 11.7–3.5 Ma and 1.4–0.1 Ma, respectively. Furthermore, due to the limited distribution of mature source rocks, each generation of petroleum migrated from the center of the sag to the edge, and the oils with lower maturity migrated for a longer period of time.

Author Contributions: Conceptualization, C.L. and H.C.; methodology, H.C.; software, C.L.; validation, H.C. and H.L.; formal analysis, C.L.; investigation, C.L. and H.C.; resources, H.L.; data curation, H.L.; writing-original draft preparation, C.L.; writing-review and editing, C.L.; visualization, C.L.; supervision, H.L.; project administration, H.L.; funding acquisition, H.L. and C.L. All authors have read and agreed to the published version of the manuscript.

Funding: This research was funded by National Basic Research Program of China, grant number 2014CB239105, and was also funded by China University of Geosciences (Wuhan), grant number cug130104.

Institutional Review Board Statement: Not applicable.

Informed Consent Statement: Not applicable.

Data Availability Statement: The data presented in this study cannot be shared at this time for some ongoing further studies.

Acknowledgments: Special thanks to the three anonymous reviewers for their valuable and constructive suggestions. This study was supported by National Basic Research Program of China (Grant No. 2014CB239105), and Fundamental Research Funds for the Central Universities, China University of Geosciences (Wuhan) (Grant No. cug130104). We appreciate their financial support. Meanwhile, thanks are given to the Key Laboratory of Tectonics and Petroleum Resources (China University of Geosciences), Ministry of Education, for all laboratory tests.

Conflicts of Interest: The authors declare no conflict of interest.

References

1. McLimans, R.K. The application of fluid inclusions to migration of oil and diagenesis in petroleum reservoirs. *Appl. Geochem.* **1987**, *2*, 585–603. [\[CrossRef\]](#)
2. Leythaeuser, D.; Rückheim, J. Heterogeneity of oil composition within a reservoir as a reflectance of accumulation history. *Geochim. Cosmochim. Acta* **1989**, *53*, 2119–2123. [\[CrossRef\]](#)
3. Nedkvitne, T.; Karlsen, D.A.; Bjørlykke, K.; Larter, S.R. Relationship between reservoir diagenetic evolution and petroleum emplacement in the Ula Field, North Sea. *Mar. Pet. Geol.* **1993**, *10*, 255–270. [\[CrossRef\]](#)
4. Mark, D.F.; Parnell, J.; Kelley, S.P.; Lee, M.; Sherlock, S.C.; Carr, A. Dating of multistage fluid flow in sandstones. *Science* **2005**, *309*, 2048–2051. [\[CrossRef\]](#) [\[PubMed\]](#)
5. Cao, J.; Jin, Z.J.; Hu, W.X.; Xie, X.M.; Wang, X.L.; Yao, S.P. Integrated GOI and composition data of oil inclusions to reconstruct petroleum charge history of gas-condensate reservoirs: Example from the Mosuowan area, central Junggar basin (NW China). *Acta Petrol. Sin.* **2007**, *23*, 137–144.
6. Shi, H.S.; Zhu, J.Z.; Qiu, H.N.; Shu, Y.; Wu, J.Y.; Long, Z.L. Timing of hydrocarbon fluid emplacement in sandstone reservoirs in Neogene in Huizhou Sag, Southern China Sea, by authigenic illite ^{40}Ar - ^{39}Ar Laser stepwise heating. *Earth Sci. Front.* **2009**, *16*, 290–295.
7. Li, C.Q.; Chen, H.H.; Liu, H.M. Identification of hydrocarbon charging events by using micro-beam fluorescence spectra of petroleum inclusions. *Earth Sci.* **2010**, *35*, 657–662, (In Chinese with English abstract).
8. Burruss, R.C.; Cercone, K.R.; Harris, P.M. Fluid inclusion petrography and tectonic-burial history of the Al Ali No.2 well: Evidence for the timing of diagenesis and oil migration, northern Oman Foredeep. *Geology* **1983**, *11*, 567–570. [\[CrossRef\]](#)
9. Parnell, J.; Carey, P.; Duncan, W. History of hydrocarbon charge on the Atlantic margin: Evidence from fluid-inclusion studies, West of Shetland. *Geology* **1998**, *26*, 807–810. [\[CrossRef\]](#)
10. Bhullar, A.G.; Karlsen, D.A.; Backer-Owe, K.; Seland, R.T.; Tran, K.L. Dating reservoir filling—A case history from the North Sea. *Mar. Pet. Geol.* **1999**, *16*, 581–603. [\[CrossRef\]](#)
11. Barclay, S.A.; Worden, R.H.; Parnell, J.; Hall, D.L.; Sterner, S.M. Assessment of fluid contacts and compartmentalization in sandstone reservoirs using fluid inclusions: An example from the Magnus oil field, North Sea. *AAPG Bull.* **2000**, *84*, 489–504.
12. Li, C.; Chen, H. Hydrocarbon Inclusion Characteristics in the Cambrian-Ordovician Carbonates of the TS2 Well: Implication for Deep Hydrocarbon Exploration in the Tahe Oilfield, Tarim Basin, Northwest China. *Acta Geol. Sin. (Engl. Ed.)* **2015**, *89*, 852–860.
13. Atwah, I.; Mohammadi, S.; Moldowan, J.M.; Dahl, J. Episodic hydrocarbon charge in tight Mississippian reservoirs of Central Oklahoma, USA: Insights from oil inclusion geochemistry. *Mar. Pet. Geol.* **2021**, *123*, 104742. [\[CrossRef\]](#)
14. Roedder, E.; Bodnar, R.J. Geologic pressure determinations from fluid inclusion studies. *Annu. Rev. Earth Planet. Sci.* **1980**, *8*, 263–301. [\[CrossRef\]](#)
15. Barker, C.E.; Goldstein, R.H. Fluid-inclusion technique for determining maximum temperature in calcite and its comparison to the vitrinite reflectance geothermometer. *Geology* **1990**, *18*, 1003–1006. [\[CrossRef\]](#)
16. Tseng, H.Y.; Pottorf, R.J. Fluid inclusion constraints on petroleum PVT and compositional history of the Greater Alwyn-South Brent petroleum system, northern North Sea. *Mar. Pet. Geol.* **2002**, *19*, 797–809. [\[CrossRef\]](#)
17. Guilhaumou, N.; Szydłowski, N.; Pradier, B. Characterization of hydrocarbon fluid inclusions by infra-red and fluorescence microspectrometry. *Mineral. Mag.* **1990**, *54*, 311–324. [\[CrossRef\]](#)
18. Pironon, J.; Canals, M.; Dubessy, J.; Walgenwitz, F.; Laplace-Builhe, C. Volumetric reconstruction of individual oil inclusions by confocal scanning laser microscopy. *Eur. J. Mineral.* **1998**, *10*, 1143–1150. [\[CrossRef\]](#)

19. Aplin, A.C.; Macleod, G.; Larter, S.R.; Pedersen, K.S.; Sorensen, H.; Booth, T. Combined use of Confocal Laser Scanning Microscopy and PVT simulation for estimating the composition and physical properties of petroleum in fluid inclusions. *Mar. Pet. Geol.* **1999**, *16*, 97–110. [[CrossRef](#)]
20. Burke, E.A.J. Raman microspectrometry of fluid inclusions. *Lithos* **2001**, *55*, 139–158. [[CrossRef](#)]
21. Thiéry, R.; Pironon, J.; Walgenwitz, F.; Motel, F. Individual characterization of petroleum fluid inclusions (composition and P-T trapping conditions) by microthermometry and confocal laser scanning microscopy: Inferences from applied thermodynamics of oils. *Mar. Pet. Geol.* **2002**, *19*, 847–859. [[CrossRef](#)]
22. Liu, K.; George, S.C.; Lu, X.; Gong, S.; Tian, H.; Gui, L. Innovative fluorescence spectroscopic techniques for rapidly characterising oil inclusions. *Org. Geochem.* **2014**, *72*, 34–45. [[CrossRef](#)]
23. Munz, I.A. Petroleum inclusions in sedimentary basins: Systematics, analytical methods and applications. *Lithos* **2001**, *55*, 195–212. [[CrossRef](#)]
24. Eadington, P.J.; Hamilton, P.J.; Bai, G.P. Fluid history analysis—A new concept for prospect evaluation. *APPEA J.* **1991**, *31*, 282–294. [[CrossRef](#)]
25. Hall, D.; Shentwu, W.; Sterner, M. Using fluid inclusions to explore for oil and gas. *Pet. Eng. Int.* **1997**, *70*, 29–34.
26. Chen, H.; Zhang, Q.; Shi, J. Evidence of fluid inclusion for thermal fluid-bearing hydrocarbon movements in Qiongdongnan Basin, South China Sea. *Sci. China Ser. D Earth Sci.* **1997**, *40*, 648–655. [[CrossRef](#)]
27. Cao, J.; Yao, S.; Jin, Z.; Hu, W.; Zhang, Y.; Wang, X.; Zhang, Y.; Tang, Y. Petroleum migration and mixing in the northwestern Junggar Basin (NW China): Constraints from oil-bearing fluid inclusion analyses. *Org. Geochem.* **2006**, *37*, 827–846. [[CrossRef](#)]
28. Bourdet, J.; Eadington, P.; Volk, H.; George, S.C.; Pironon, J.; Kempton, R. Chemical changes of fluid inclusion oil trapped during the evolution of an oil reservoir: Jabiru-1A case study (Timor Sea, Australia). *Mar. Pet. Geol.* **2012**, *36*, 118–139. [[CrossRef](#)]
29. Volk, H.; George, S.C. Using petroleum inclusions to trace petroleum systems—A review. *Org. Geochem.* **2019**, *129*, 99–123. [[CrossRef](#)]
30. Han, Y.; Noah, M.; Lüders, V.; Hartwig, A.; Rinna, J.; Skeie, J.E.; Horsfield, B.; Mangelsdorf, K. Geochemical characteristics of inclusion oils from the Skarv field A segment and their implications for the oil charge and leakage history. *Mar. Pet. Geol.* **2022**, *137*, 105506. [[CrossRef](#)]
31. Cai, L.; Chen, H.; Li, C.; Li, Z.; Liu, H.; Hao, X. Reconstruction of paleo-fluid potential field of Es³ in the Dongying sag of the Jiyang depression with systematic fluid inclusion analysis. *Oil Gas Geol.* **2009**, *30*, 17–25, (In Chinese with English abstract).
32. Liu, H.M. Pressure response to hydrocarbon charging events in Es₃ Member of Minfeng sub-sag. *Xinjiang Pet. Geol.* **2009**, *30*, 483–485, (in Chinese with English abstract).
33. Ping, H.; Chen, H.; Jia, G. Petroleum accumulation in the deeply buried reservoirs in the northern Dongying Depression, Bohai Bay Basin, China: New insights from fluid inclusions, natural gas geochemistry, and 1-D basin modeling. *Mar. Pet. Geol.* **2017**, *80*, 70–93. [[CrossRef](#)]
34. Wang, Y.; Hao, X.; Hu, Y. Orderly distribution and differential enrichment of hydrocarbon in oil-rich sags: A case study of Dongying Sag, Jiyang Depression, Bohai Bay Basin, East China. *Pet. Explor. Dev.* **2018**, *45*, 840–850. [[CrossRef](#)]
35. Zhu, J.C.; Zou, C.N.; Feng, Y.L.; Jiang, S.; Wu, W.A.; Zhu, R.X.; Yuan, M. Distribution and controls of petroliferous plays in subtle traps within a Paleogene lacustrine sequence stratigraphic framework, Dongying Depression, Bohai Bay Basin, Eastern China. *Pet. Sci.* **2020**, *17*, 1–22. [[CrossRef](#)]
36. Hu, J.Y.; Xu, S.B.; Tong, X.G.; Wu, H.Y. The Bohai Bay Basin. In *Chinese Sedimentary Basins*; Zhu, X., Ed.; Elsevier: Amsterdam, The Netherlands, 1989; pp. 89–105.
37. Chang, C.Y. Geological characteristics and distribution patterns of hydrocarbon deposits in the Bohai Bay Basin, east China. *Mar. Pet. Geol.* **1991**, *8*, 98–106. [[CrossRef](#)]
38. Allen, M.B.; Macdonald, D.I.M.; Xun, Z.; Vincent, S.J.; Brouet-Menzies, C. Early Cenozoic two-phase extension and late Cenozoic thermal subsidence and inversion of the Bohai Basin, northern China. *Mar. Pet. Geol.* **1997**, *14*, 951–972. [[CrossRef](#)]
39. Hu, S.; O’Sullivan, P.B.; Raza, A.; Kohn, B.P. Thermal history and tectonic subsidence of the Bohai Basin, northern China: A Cenozoic rifted and local pull-apart basin. *Phys. Earth Planet. Inter.* **2001**, *126*, 221–235. [[CrossRef](#)]
40. Chen, J.; Li, S.; Xiong, Y.; Bi, Y. Multiple petroleum systems in Tertiary extensional basins, east China: A case study of the Gunan-Fulin Basin. *J. Pet. Geol.* **1998**, *21*, 105–118.
41. Wu, L.; Xu, H.M.; Ji, H.C. Evolution of sedimentary system and analysis of sedimentary source in Paleogene of the Bozhong sag, Bohai Bay. *Mar. Geol. Quat. Geol.* **2006**, *26*, 81–88, (In Chinese with English abstract).
42. Xiao, G.L.; Chen, J.W. Oil and gas in Neogene of the Bohai Sea area. *Mar. Geol. Lett.* **2003**, *19*, 1–6, (In Chinese with English abstract).
43. Gong, Z.S. Neotectonics and petroleum accumulation in offshore Chinese basins. *Earth Sci.* **2004**, *29*, 513–517, (In Chinese with English abstract).
44. Liu, H.; Jiang, Y.L.; Ren, J.L. Characteristics of petroleum system and oil-source in Dongying depression. *Geol. J. China Univ.* **2009**, *15*, 93–99, (In Chinese with English abstract).
45. Van den Kerkhof, A.M.; Hein, U.F. Fluid inclusion petrography. *Lithos* **2001**, *55*, 27–47. [[CrossRef](#)]
46. Goldstein, R.H.; Reynolds, T.J. *Systematics of Fluid Inclusions in Diagenetic Minerals*; Short course 31; SEPM: Tulsa, OK, USA, 1994; pp. 69–85.

47. Chi, G.; Diamond, L.W.; Lu, H.; Lai, J.; Chu, H. Common problems and pitfalls in fluid inclusion study: A review and discussion. *Minerals* **2021**, *11*, 7. [[CrossRef](#)]
48. Goldstein, R.H. Fluid inclusions in sedimentary and diagenetic systems. *Lithos* **2001**, *55*, 159–193. [[CrossRef](#)]
49. Bodnar, R.J. Introduction to fluid inclusions. In *Fluid Inclusions: Analysis and Interpretation*; Short Course 32; Samson, I., Anderson, A., Marshall, D., Eds.; Mineral. Assoc.: Wolfville, NS, Canada, 2003; pp. 1–8.
50. Guo, X.; He, S.; Liu, K.; Song, G.; Wang, X.; Shi, Z. Oil generation as the dominant overpressure mechanism in the Cenozoic Dongying depression, Bohai Bay Basin, China. *AAPG Bull.* **2010**, *94*, 1859–1881. [[CrossRef](#)]
51. Ratnayake, A.S.; Kularathne, C.W.; Sampei, Y. Assessment of hydrocarbon generation potential and thermal maturity of the offshore Mannar Basin, Sri Lanka. *J. Pet. Explor. Prod. Technol.* **2018**, *8*, 641–654. [[CrossRef](#)]
52. Ratnayake, A.S.; Sampei, Y. Characterization of organic matter and depositional environment of the Jurassic small sedimentary basins exposed in the northwest onshore area of Sri Lanka. *Res. Org. Geochem.* **2015**, *31*, 15–28.
53. Hagemann, H.W.; Hollerbach, A. The fluorescence behaviour of crude oils with respect to their thermal maturation and degradation. *Org. Geochem.* **1986**, *10*, 473–480. [[CrossRef](#)]
54. Stasiuk, L.D.; Snowdon, L.R. Fluorescence micro-spectrometry of synthetic and natural hydrocarbon fluid inclusions: Crude oil chemistry, density and application to petroleum migration. *Appl. Geochem.* **1997**, *12*, 229–241. [[CrossRef](#)]
55. Chang, Y.J.; Huang, W.L. Simulation of the fluorescence evolution of “live” oils from kerogens in a diamond anvil cell: Application to inclusion oils in terms of maturity and source. *Geochim. Cosmochim. Acta* **2008**, *72*, 3771–3787. [[CrossRef](#)]
56. Zhao, Y.J.; Chen, H.H. The relationship between fluorescence colors of oil inclusions and their maturities. *Earth Sci.* **2008**, *33*, 91–96, (In Chinese with English abstract).
57. George, S.C.; Ruble, T.E.; Dutkiewicz, A.; Eadington, P.J. Assessing the maturity of oil trapped in fluid inclusions using molecular geochemistry data and visually-determined fluorescence colours. *Appl. Geochem.* **2001**, *16*, 451–473. [[CrossRef](#)]
58. Oxtoby, N.H. Comments on: Assessing the maturity of oil trapped in fluid inclusions using molecular geochemistry data and visually-determined fluorescence colours. *Appl. Geochem.* **2002**, *17*, 1371–1374. [[CrossRef](#)]
59. George, S.C.; Ruble, T.E.; Dutkiewicz, A.; Eadington, P.J. Reply to comment by Oxtoby on “Assessing the maturity of oil trapped in fluid inclusions using molecular geochemistry data and visually-determined fluorescence colours”. *Appl. Geochem.* **2002**, *17*, 1375–1378. [[CrossRef](#)]
60. Chen, H. Microspectrofluorimetric characterization and thermal maturity assessment of individual oil inclusion. *Acta Pet. Sin.* **2014**, *35*, 584–590, (In Chinese with English abstract).
61. Ping, H.; Chen, H.; George, S.C.; Li, C.; Hu, S. Relationship between the fluorescence color of oil inclusions and thermal maturity in the Dongying Depression, Bohai Bay Basin, China: Part 1. Fluorescence evolution of oil in the context of hydrous pyrolysis experiments with increasing maturity. *Mar. Pet. Geol.* **2019**, *100*, 1–19. [[CrossRef](#)]
62. Ping, H.; Chen, H.; George, S.C.; Li, C.; Hu, S. Relationship between the fluorescence color of oil inclusions and thermal maturity in the Dongying Depression, Bohai Bay Basin, China: Part 2. fluorescence evolution of oil in the context of petroleum generation, expulsion and cracking under geological conditions. *Mar. Pet. Geol.* **2019**, *103*, 306–319.
63. Bertrand, P.; Pittion, J.; Bernaud, C. Fluorescence of sedimentary organic matter in relation to its chemical composition. *Org. Geochem.* **1986**, *10*, 641–647. [[CrossRef](#)]
64. Kularathna, E.K.C.W.; Pitawala, H.M.T.G.A.; Senaratne, A.; Ratnayake, A.S. Play distribution and the hydrocarbon potential of the Mannar Basin, Sri Lanka. *J. Pet. Explor. Prod. Technol.* **2020**, *10*, 2225–2243. [[CrossRef](#)]
65. Jiang, Y.; Zhuo, Q.; Tan, Y.; Lu, X. Diversity in the thermal evolution and hydrocarbon generation of source rocks in different sub-depressions of rich oil depression. *Pet. Geol. Exp.* **2009**, *31*, 500–505.